International Journal of Multiphase Flow 36 (2010) 40–50

Contents lists available at ScienceDirect

International Journal of Multiphase Flow

journal homepage: www.elsevier.com/locate/ijmulflow

Simulation of large amplitude waves in a slug tracking scheme compared to roll wave experiments at high pressure

A. De Leebeeck *, O.J. Nydal

Department of Energy and Process Engineering, Norwegian University of Science and Technology, NO-7491 Trondheim, Norway

ARTICLE INFO

Article history:
Received 18 April 2009
Received in revised form 2 September 2009
Accepted 3 September 2009
Available online 8 September 2009

Keywords:
Slug tracking scheme
Roll waves
Two-phase flow
Numerical simulation

ABSTRACT

Due to the similarities between large amplitude roll waves and slug flow in two-phase gas–liquid pipe flow, a slug tracking scheme is presented with the addition of a simplified model for roll waves. The waves are treated in a similar way to slugs, modelled as objects moving at the wave velocity and with a pressure variation across them. The two-fluid model is solved on a stationary staggered grid in stratified sections between moving waves and slugs. The model is dynamic meaning that the growth and decay of waves and slugs can be simulated. The wave model implementation within the tracking scheme is discussed and demonstrated in comparison to existing experimental data on wave velocities and averaged pressure drops. The results from the tracking scheme compared well to the experiments when waves were initiated with the experimental frequency. Wave initiation remains as a modelling challenge.

1. Background

In two-phase gas–liquid pipe flow, different flow regimes occur depending on gas and liquid phase velocities, fluid properties, and pipe geometries. Various numerical strategies exist for the modelling of flow regimes at different scales. Slug flow and flow with large amplitude waves can be treated in an averaged manner using repeating unit cells (Bendiksen et al., 1996; Johnson, 2005) assuming steady, fully developed flow. The steady state roll wave model of Johnson (2005) assumes a sequence of repeating "maximum amplitude" waves with a sharp front and includes a unique interface friction factor accounting for increased friction in wavy flows. Unit cell methods give adequate predictions of average holdup and pressure drop but do not include slug or wave dynamics such as growth or decay. Johnson's (2005) model gives more information about the waves such as their velocity, amplitude and the length from one wave peak to the next in addition to average holdup and pressure drop but does not include wave dynamics. Alternatively, slugs and waves can be resolved individually in capturing (Andreussi et al., 2008; Bonizzi and Issa, 2003; Issa and Kempf, 2003; Renault, 2007; Holmås, 2008) or tracking (Taitel and Barnea, 1998; Nydal and Banerjee, 1996; Kjølaas, 2007; Hu et al., 2007) schemes.

Capturing techniques use a two-fluid model on a fine grid much smaller than the characteristic slug length to model slug flow (Renault, 2007; Issa and Kempf, 2003; Bonizzi and Issa, 2003) or flow with large amplitude waves (Holmås, 2008). Slug or wave initiation can be captured but the required refined grid becomes computationally expensive in long pipe systems. Holmås's (2008) model, however, uses a more efficient numerical method, the pseudo-spectral Fourier method, to capture the growth of roll waves but the solution breaks down for slug flow.

Tracking schemes are preferred for this work because coarser grids are possible, reducing the computational expense associated with more refined grids. In a tracking scheme, stratified sections between slugs are modelled on a coarse fixed grid while slugs are modelled as moving objects. Slugs, or similar moving objects, have boundaries corresponding to sharp fronts thus avoiding numerical diffusion and the need for excessive grid refinement (Kjølaas, 2007). Front physics such as bubble nose velocities or gas entrainment can also be implemented. Tracking schemes have also been tested for plug simulations where plugs are treated as rigid moving objects (Kjølaas, 2007). A combination of capturing for slug initiation and tracking has also been tested (Renault, 2007). The slug tracking scheme of Hu et al. (2007) includes the liquid height profile (tail) behind waves and slugs, solving the two-fluid model in combination with modelling the wave front as a hydraulic jump.

Flow with large amplitude roll waves shows some similarities to slug flow (De Leebeeck et al., 2007; Lin and Hanratty, 1987; Hanyang and Liejin, 2008) which would suggest that roll waves can be incorporated into a tracking scheme in similar fashion to slugs. These similarities include transport of liquid, a propagation velocity, sharp fronts and a sloping tail (Johnson, 2005; Ottens et al., 2001; Hanyang and Liejin, 2008; Soleimani and Hanratty, 2003; Andritsos and Hanratty, 1987). Measurements also suggest that waves have a pressure variation across them due to

* Corresponding author. Tel.: +47 73593898; fax: +47 73593580.
E-mail address: angela.de.leebeeck@ntnu.no (A. De Leebeeck).

0301-9322/$ - see front matter © 2009 Elsevier Ltd. All rights reserved.
doi:10.1016/j.ijmultiphaseflow.2009.09.002

acceleration of liquid at the wave front (De Leebeeck et al., 2007). The focus of this work, therefore, is on a tracking scheme including the problem of large amplitude roll waves. To accomplish this an integral wave model and continuous transitions between slug, wave and stratified flow are needed.

In this work, a simple model for roll waves as moving objects similar to slugs has been incorporated in an existing slug tracking scheme following the latest implementation by Kjølaas (2007). Experiments that have measured wave speed and pressure variation across waves (De Leebeeck et al., 2007; De Leebeeck and Nydal, 2009) have formed the basis for modelling waves as moving objects with an associated pressure variation. A simple model for wave velocity is suggested, allowing for transition to and from slug flow and we propose to model gas flow and pressure variation over a large wave as similar to gas flow through an orifice. The wave tracking scheme is then demonstrated by comparing to experimental data on wave velocity and averaged pressure drop in roll waves (Johnson, 2005).

2. Model description

The wave model is an addition to an existing slug tracking code following the latest implementation by Kjølaas (2007). In Kjølaas's (2007) implementation of the scheme, the two-fluid model is solved in stratified sections and hydrate plug tracking capabilities have been added. The tracking concept is now applied to other moving objects in the pipe, roll waves. The numerical model for slugs on a moving grid and stratified regions on a stationary grid has already been developed (Kjølaas, 2007) but is reviewed here to show how the simplified wave tracking model has been incorporated with the existing scheme. The model for slugs implemented by Kjølaas (2007) and the model for waves implemented here are summarized in Tables 1 and 2, respectively.

The wave and slug tracking scheme uses a one-dimensional finite volume method and applies to two-phase gas–liquid flow in a pipe. For the purposes of wave tracking, flow is assumed isothermal so the energy equation can be neglected. It is also assumed that there is no mass transfer between the phases through evaporation or condensation. Gas entrainment can be included in slugs but is not modelled in stratified regions or waves. Droplets in the gas phase are also neglected.

2.1. Geometry

Pipeline geometry is listed as a sequence of pipes with a length, angle of inclination, internal diameter, and roughness for

Table 1
Slug model summary.

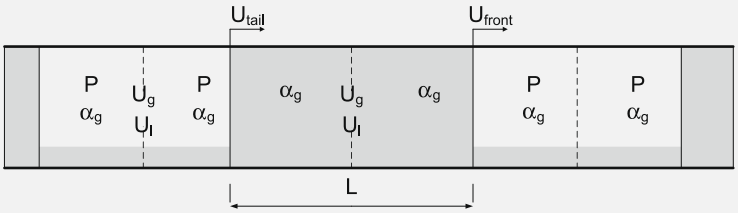

Slug sections	U_l	Mixture momentum balance equation (8)
	U_g	Slip relation equation (9)
	α_g	Gas entrainment correlation, if any
	L	Mass balance equations (22) and (23)
Stratified sections	P	Equations of state (5)
	α_g	Mass balance equation (7)
	U_l	Liquid momentum equation (4)
	U_g	Gas momentum equation (4)
Borders	U_{tail}	Bubble nose or slug tail velocity equation (11)
	U_{front}	Mass balance across slug front equation (10)

Table 2
Wave model summary.

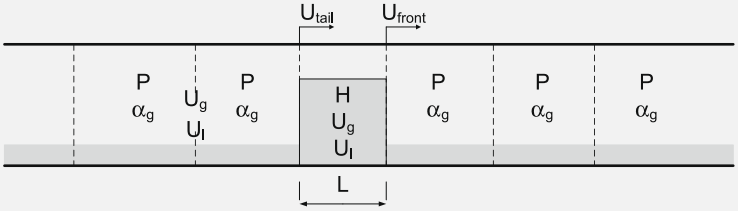

Wave sections	U_l	Liquid momentum balance equation (19) with front acceleration, friction, gravity and pressure drop
	U_g	Gas momentum balance equation (18) with orifice type loss, gravity and pressure drop
	H	Mass balance equations (22) and (23)
	L	Fixed length of wave front
Stratified sections	P	Equations of state (5)
	α_g	Mass balance equation (7)
	U_l	Liquid momentum equation (4)
	U_g	Gas momentum equation (4)
Borders	$U_{tail} = 1.2U_l$	Continuous to bubble nose velocity when $H = 1$, Eq. (21)
	U_{front}	Mass balance across wave front, Eq. (20)

calculating the frictional shear stress at the pipe walls. The pipeline can consist of one or more pipes of varying length and/or inclination, and include bends. At the boundaries between two pipes (bends) mass is free to flow in either direction.

2.2. Fluid properties

For wave tracking, the ideal gas law is used to determine the gas density. Other fluid properties such as viscosities, liquid density, and the molecular mass of the gas phase are specified by the user. The constant temperature of the fluids and outlet, inlet and initial pressure are specified so that the gas density can be calculated from the ideal gas law. The only reason for specifying the inlet pressure is so that the gas density at the inlet can be determined. It does not have any other mechanical consequences. Inside the pipe, gas density varies according to the simulated pressure.

2.3. Grids and time steps

The sequence of pipes is divided into sections including stratified sections, slug sections, and large roll wave sections. The sections are the computational grid. The boundary between a section and its neighbor is termed the section border. Since the grid is dynamic, three grid sizes are specified: a maximum and minimum grid size for stratified sections, and a minimum grid size for slugs around 1 or 2 pipe diameters. When a stratified section exceeds maximum length it is split into two smaller sections, or merged with a neighboring section if it is less than the minimum length. When slugs reach minimum length they decay to waves. The wave front is modelled as an object with a short fixed length equal to the minimum slug length.

In stratified sections, the gas and liquid phases are separate and the two-fluid model is solved on a stationary staggered grid. In the staggered grid arrangement, phase velocities are determined at section borders, while pressure, area fraction, and other quantities are determined at section centers. The staggered arrangement avoids checkerboard oscillations that would occur if pressure and velocities were determined at the same location (Ferziger and Perić, 2001).

Slug and wave sections, however, are modelled with moving borders. These section borders move with a border velocity and their position is updated at each time step. The border velocities are greater than the liquid phase velocity in stratified sections. Liquid slug sections completely fill the pipe and they may or may not contain entrained gas depending on the modelling of the gas entrainment rate at the slug front. Slug front and tail borders move with separate velocities allowing the slug to grow or shrink in length. Wave fronts are modelled in similar fashion to slugs, except gas is allowed to flow over them and they have a fixed length. The wave moves at the wave front velocity and if the wave tail velocity is different from the front velocity, the holdup in the wave front will either increase or decrease according to the mass balance over the front. Thus the wave grows or decays in amplitude.

Fig. 1 illustrates the spatial index convention used in stratified sections and slugs. The convention for slugs is also applied to waves. In stratified sections, index J represents the section center indicated with a dashed line while index j indicated with a solid line is the border to the left of section J. In moving slugs and waves, index j is the center of the slug or wave (dashed line) while index J is its right border (solid line).

Start and end times as well as the desired simulation time step are given by the user. Time steps are indicated by superscripts where n represents the current time step and $n+1$ represents the next time step. Quantities with superscript n are known at the current time step while those with superscript $n+1$ need to be determined.

2.4. Friction models

Frictional shear stress at the wall is expressed using a friction factor as follows:

$$\tau = \frac{1}{8}\lambda\rho|U|U \tag{1}$$

where τ is the shear stress, ρ is the phase density, U is the phase velocity, and λ is the Darcy friction factor.

The shear stress at the interface, τ_i, for smooth stratified flow is normally written as:

$$\tau_i = \frac{1}{8}\lambda_g\rho_g|U_g - U_l|(U_g - U_l) \tag{2}$$

where λ is the Haaland friction factor (Haaland, 1983) for phase k determined from:

$$\frac{1}{\sqrt{\lambda_k}} = -1.8\log\left(\frac{6.9}{Re_k} + \left(\frac{\epsilon}{3.7D_{h,k}}\right)^{1.11}\right) \tag{3}$$

where Reynolds number for phase k is $Re_k = \rho_k D_{h,k} U_k/\mu_k$, μ is the viscosity, and ϵ is the pipe wall roughness. Phase k can be either liquid indicated by subscript l or gas, subscript g. Hydraulic diameters D_h for the gas phase and liquid phase are:

$$\text{Gas phase} \quad D_{h,g} = \frac{\pi D^2}{S_g + S_i}$$

$$\text{Liquid phase} \quad D_{h,l} = \frac{\pi D^2}{S_l}$$

where S_g and S_l are the wetted wall perimeters and S_i is the interface length. D is the pipe diameter.

2.5. Two-fluid equations for stratified flow sections

In stratified sections, the two-fluid model consisting of the gas and liquid momentum equations, the pressure equation, and the gas and liquid mass balance equations are solved on a staggered grid adopting the notation as shown in Fig. 1. The discretized version of these equations as in Kjølaas (2007) are reviewed. For the

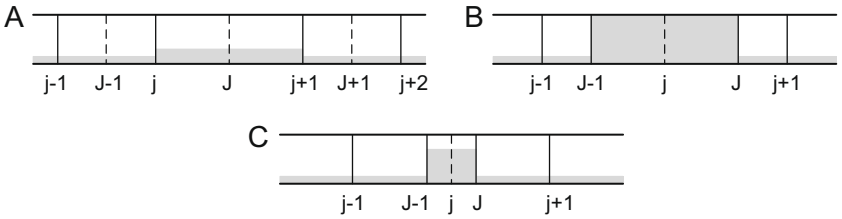

Fig. 1. Index notation in (A) stratified sections, (B) slug sections, and similar to slugs, (C) wave sections. Solid lines represent section borders, while dotted lines mark section centers.

differential form of the mass, momentum and pressure equations before discretization, see Electronic Annex 1.

The discretized momentum balance equation for phase k is given as:

$$M_{k,j}^n \frac{\Delta U_k}{\Delta t} + m_{k,J}^n A\left(U_{k,J}^n - U_{b,J}^n\right)\left(\widehat{U}_{k,J}^{n+1} - U_{k,j}^{n+1}\right) - m_{k,J-1}^n A\left(U_{k,J-1}^n - U_{b,J-1}^n\right) \times \left(\widehat{U}_{k,J-1}^{n+1} - U_{k,j}^{n+1}\right) = -\alpha_{k,j}^n A\left(P_J^{n+1} - P_{J-1}^{n+1}\right) - M_{k,j}^n g\cos\theta \frac{h_{l,J}^n - h_{l,J-1}^n}{L_j^n} - \frac{1}{8} S_{k,j}^n L_j^n \lambda_{k,j}^n \rho_{k,j}^n |U_{k,j}^n| \left(U_{k,j}^{n+1}\right) - \frac{1}{8} S_{i,j}^n L_j^n \lambda_{i,j}^n \rho_{g,j}^n |U_{k,j}^n - U_{n,j}^n| \left(U_{k,j}^{n+1} - U_{n,j}^{n+1}\right) - M_{k,j}^n g\sin\theta \quad (4)$$

where M is the phase mass, $\Delta U_k = U_k^{n+1} - U_k^n$, Δt is the time step size, $m = M/AL$ is the phase specific mass, A is the pipe cross-sectional area, S is the wetted wall perimeter, t is time, α is the area fraction, P is pressure, L is the section length, h_l is the liquid height, g is the acceleration of gravity (9.81 m/s^2), and θ is the angle of pipe inclination from the horizontal. A positive angle indicates upward inclination. The subscript b indicates a quantity associated with a border, subscript k indicates the current phase, subscript n indicates the neighboring phase, and subscript i indicates a quantity associated with the interface. Upwind discretization is used for the convection terms. Upwind quantities are indicated with a hat, e.g., the velocity $\widehat{U}_{k,J}^{n+1}$ in the above equation.

The implementation of the two-fluid model in stratified regions means that the convection terms, the second and third terms in Eq. (4), are included. This in turn means that the gradually sloping liquid height profile (tail) behind wave fronts and slugs can be resolved on a sufficiently refined grid.

The following equation, the pressure equation, is a combination of the mass balance and equations of state for both phases:

$$\sum_k \frac{V_{k,J}^n}{\rho_{k,J}^n}\left[\left(\frac{\partial\rho_{k,J}^n}{\partial P}\right)_{T_k} \frac{P_J^{n+1} - P_J^n}{\Delta t}\right] + A\left(U_{b,j+1}^{n+1} - U_{b,j}^{n+1}\right) + \sum_k \frac{1}{\rho_{k,J}^n}\left[\hat{m}_{k,j+1}^n A\left(U_{k,j+1}^{n+1} - U_{b,j+1}^{n+1}\right) - \hat{m}_{k,j}^n A\left(U_{k,j}^{n+1} - U_{b,j}^{n+1}\right)\right] = \psi_{s,J} \quad (5)$$

where V is volume, T is temperature, and $\left(\frac{\partial\rho_{k,J}^n}{\partial P}\right)_{T_k}$ is determined from the ideal gas law. The pressure equation (5) is solved simultaneously with the momentum balance equation (4) to get phase velocities defined at section borders and pressure defined at the center of stratified sections. The model can work with either an incompressible or a compressible liquid in stratified flow. When single phase liquid occurs, as in a slug, the computational domain is divided into compressible and incompressible regions. This avoids the problem of having one universal scheme to work for both compressible and incompressible cases.

The volume error term $\psi_{s,J}$ in Eq. (5) is defined as follows:

$$\psi_{s,J} = \frac{V_J}{\Delta t}\left(\sum_k \frac{m_{k,J}}{\rho_{k,J}} - 1\right) \quad (6)$$

It is included because the pressure equation is not formulated in a mass conserving manner (Kjølaas, 2007; Ferziger and Perić, 2001; Prosperetti and Tryggvason, 2007) and the use of the staggered grid can introduce a first order error from acceleration by a body force (Fletcher and Thyagaraja, 1991). Including the volume error term ensures consistency between pressure and mass over time, without iteration.

The discretized mass balance equation uses an implicit time integration which is more robust for longer time steps. Mass is determined at the centers of stratified sections using the following equation:

$$\frac{\Delta M_{k,J}}{\Delta t} + \frac{\widehat{M}_{k,j+1}^{n+1}}{\widehat{L}_{j+1}^n}\left(U_{k,j+1}^{n+1} - U_{b,j+1}^{n+1}\right) - \frac{\widehat{M}_{k,j}^{n+1}}{\widehat{L}_j^n}\left(U_{k,j}^{n+1} - U_{b,j}^{n+1}\right) = 0 \quad (7)$$

The mass balance equations are solved after the pressure equation and the phase fractions are determined from the masses and densities at the new pressure. As the phase fractions may not sum to unity, the phase fractions are normalized and the error term is introduced as a source term in the pressure equation (5). Including the error term in the pressure equation allows the equations to be solved non-iteratively and reduces the computational cost, and the implicit formulation ensures stability (Kjølaas, 2007).

2.6. Slugs

The dynamics of the flow in a slug can be determined from a mixture momentum equation and a slip relation. A simplified version of the mixture momentum equation is the liquid equation without the gas interaction term. The discretized version of the liquid momentum equation in slugs takes a similar form to Eq. (4), except interface friction can be neglected (no interface), as follows:

$$M_{l,j}^n \frac{\Delta U_l}{\Delta t} + m_{l,J}^n A\left(U_{l,J}^n - U_{b,J}^n\right)\left(\widehat{U}_{l,J}^{n+1} - U_{l,j}^{n+1}\right) - m_{l,J-1}^n A\left(U_{l,J-1}^n - U_{b,J-1}^n\right)\left(\widehat{U}_{l,J-1}^{n+1} - U_{l,j}^{n+1}\right) = -H_j^n A\left(P_J^{n+1} - P_{J-1}^{n+1}\right) - \frac{1}{8} S_{l,j}^n L_j^n \lambda_{l,j}^n \rho_{l,j}^n |U_{l,j}^n| \left(U_{l,j}^{n+1}\right) - M_{l,j}^n g\sin\theta \quad (8)$$

The second and third terms in Eq. (8) account for pressure variation due to acceleration of the liquid in the slug front.

Gas velocity in a slug is determined using a slip relation or assuming no slip:

$$U_{g,slug} = S_d(U_{l,slug} + v_o) \quad (9)$$

In the simplest case of no slip, the distribution slip ratio S_d is unity and the averaged drift velocity v_o is zero.

The slug front velocity is determined from a mass balance across the front, as follows:

$$U_{front} = \frac{H_{slug}U_{l,slug}^{n+1} - H_{bubble}U_{l,bubble}^n}{H_{slug} - H_{bubble}} \quad (10)$$

where H is liquid holdup, the subscript *slug* indicates quantities associated with the slug while subscript *bubble* indicates quantities belonging to the stratified section neighboring the slug. For the case of a slug without gas entrainment, the holdup H_{slug} goes to 1 and the local mixture velocity in a slug goes to the liquid velocity $U_{l,slug}$.

Slug tail or bubble nose velocity is determined using the following equation, proposed by Bendiksen et al. (1996) and Bendiksen (1984):

$$U_{tail} = C_o U_{mix} + U_o \quad (11)$$

where $U_{mix} = H_{slug}U_{l,slug} + (1 - H_{slug})U_{g,slug}$ is the local mixture velocity in the slug. Values for C_o and U_o which give the largest U_{tail} are applied, as follows:

$C_o = 1.05 + 0.15\sin^2\theta$	$U_o = U_{ov} + U_{oh}$	if $\lvert U_{mix}\rvert < 3.6\sqrt{gD}/\cos\theta$
$C_o = 1.2$	$U_o = U_{ov}$	if $\lvert U_{mix}\rvert > 3.6\sqrt{gD}/\cos\theta$
$U_{ov} = 0.35\sqrt{gD}\sin\theta$	$U_{oh} = \pm 0.54\sqrt{gD}\cos\theta$	

A summary of the slug model and the quantities determined is given in Table 1.

2.7. Waves

The wave model includes a pressure variation across the wave front due to liquid acceleration at the front as observed experimentally (De Leebeeck et al., 2007). The overlapped holdup

and pressure time traces corresponding to a video snapshot of a wave are plotted as an example in Fig. 2. The snapshot comes from an experiment where air and water are flowing in a 0.06 m internal diameter horizontal pipe at atmospheric conditions with superficial gas velocity $U_{sg} = 5.89$ m/s and superficial liquid velocity $U_{sl} = 0.17$ m/s. The typical wave velocities and pressure variations observed in waves during this experiment were 1.86 m/s and 1400 Pa, respectively (De Leebeeck et al., 2007).

In the wave model, it is assumed that pressures in both gas and liquid phase are equal. For a known pressure variation, the liquid phase velocity in the wave front can be determined from the liquid momentum balance equation. The gas phase however needs its own model: gas flow over a large wave can be thought of as similar to gas flow through an orifice. A schematic of a large wave compared to an orifice plate is shown in Fig. 3. The adaptation of a single phase orifice relation to gas flow over a large roll wave follows.

Starting with the single phase gas velocity through the throat of an orifice, as in the following equation (White, 2005), the orifice relation is adapted to wave flow:

$$U_t = C_d A_t \left(\frac{2\Delta P_{orifice}/\rho}{1 - \left(A_t/A_{pipe}\right)^2} \right)^{\frac{1}{2}} \tag{12}$$

where C_d is the discharge coefficient, A_t is the orifice throat area, $\Delta P_{orifice}$ is the pressure variation across the orifice, and A_{pipe} is the pipe cross-sectional area.

Rewriting Eq. (12) to give the pressure variation across the orifice gives the following:

$$\Delta P_{orifice} = \frac{1}{2}\frac{1}{C_d^2}\rho U_t^2 (1 - (A_t/A_{pipe})^2) \tag{13}$$

In thinking of gas flowing over a large wave front as similar to gas flow through an orifice, the following modifications are made to the orifice relation in Eq. (13):

$$U_t \Rightarrow U_{g,wave} - U_{front} \tag{14}$$

$$U_t^2 \Rightarrow (U_{g,wave} - U_{front})|U_{g,wave} - U_{front}| \tag{15}$$

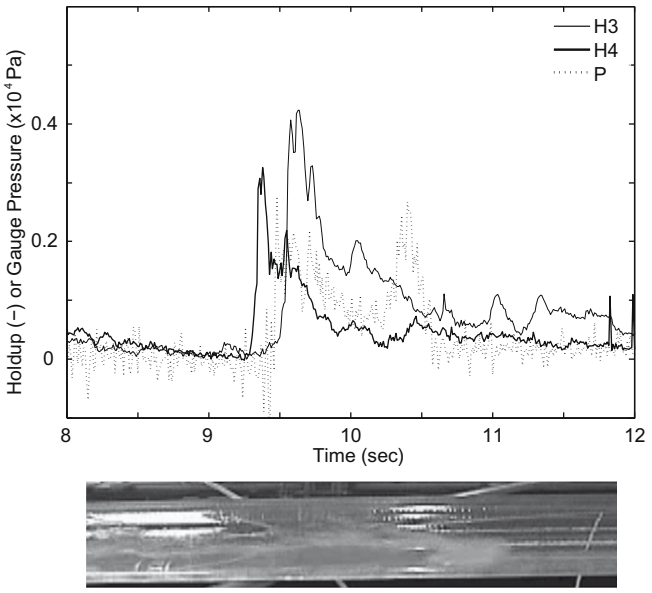

Fig. 2. Experimental pressure and holdup time traces, and corresponding image of an individual wave from air/water experiments at atmospheric pressure, horizontal pipe, $U_{sg} = 5.89$ m/s, $U_{sl} = 0.17$ m/s. The locations of holdup probes *H*3 and *H*4 and the pressure transducer *P* are 11.88 m, 14.39 m, and 13.67 m from the inlet of the pipe, respectively (De Leebeeck et al., 2007).

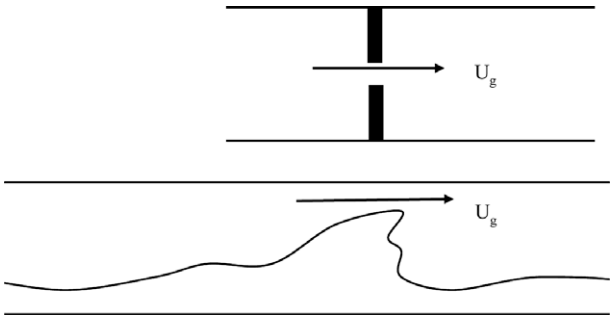

Fig. 3. Schematic of gas flow through an orifice plate (top) compared to gas flow over a large wave (bottom).

The wave is no longer stationary so U_t is replaced with the difference between the gas phase velocity over the wave $U_{g,wave}$ and the velocity of the wave front U_{front}.

The orifice relation is for single phase flow where the gas occupies the entire pipe cross section. In the case of two-phase flow, the gas phase occupies only a fraction of the pipe. In Eq. (13), the term A_{pipe} is replaced with the gas phase area ahead of the wave front $A_{g,bubble}$. The area of the orifice throat can be thought of as the area occupied by the gas at the wave front $A_{g,wave}$. The ratio of the two areas can then be written in terms of gas or liquid area fractions, as follows:

$$\frac{A_t}{A_{pipe}} \Rightarrow \frac{A_{g,wave}}{A_{g,bubble}} = \frac{A_{g,wave}/A_{pipe}}{A_{g,bubble}/A_{pipe}} = \frac{1 - H_{wave}}{1 - H_{bubble}} \tag{16}$$

where H_{wave} is the holdup in the wave front.

Finally the corresponding pressure loss to be added in the gas momentum equation for a wave is written as follows:

$$\Delta P_{wave} = \left[\frac{1}{2}\frac{1}{C_d^2}\rho_g \left(1 - \left(\frac{1 - H_{wave}}{1 - H_{bubble}} \right)^2 \right) (U_{g,wave} - U_{front})|U_{g,wave} - U_{front}| \right] \tag{17}$$

Empirical relations for the discharge coefficient C_d have been determined, depending on the ratio of the orifice throat to pipe diameter, Reynolds number, and the type of taps (corner taps or flanges for example) in the orifice (White, 2005). The typical range of values for C_d is from 0.59 to 0.66 (White, 2005) in an orifice. Since there are some differences between an actual orifice and a wave front, the question then is what should C_d be for the case of a wave? Various values of C_d can be used in simulations and compared to experimental data on waves. From there an optimal value of C_d for waves can be determined. Experimental measurements of pressure variation across a wave front (De Leebeeck et al., 2007; De Leebeeck and Nydal, 2009) led to an estimate of the discharge coefficient in the range of 0.2–0.4. These values may be lower than $C_d = 0.6$ in an actual orifice because of increased losses in the wave such as increased roughness on the wave's surface or losses due to droplet formation and air entrainment in the wave front.

The orifice type relation replaces the gas wall and interfacial shear stresses as a loss term. The following gas momentum equation for a wave front is used to determine the gas velocity by relating it to the pressure variation across the wave front:

$$\begin{aligned} &\frac{M_{g,wave}}{\Delta t}\Delta U_{g,wave} + (1 - H_{wave})A\frac{1}{2}\frac{1}{C_d^2}\rho_{g,wave}\left(1 - \left(\frac{1 - H_{wave}}{1 - H_{bubble}}\right)^2\right) \\ &\quad \times \cdot (U_{g,wave} - U_{front})|U_{g,wave} - U_{front}| \\ &= (1 - H_{wave})A(P_{J-1} - P_J) - M_{g,wave} g \sin\theta \end{aligned} \tag{18}$$

Using the same pressure variation $(P_{J-1} - P_J)$ as in Eq. (18), the following liquid momentum balance equation is used to determine the liquid phase velocity in a wave front:

$$\frac{M_{l,wave}}{\Delta t}\Delta U_{l,wave} + H\rho_{l,wave}A(U^n_{l,wave} - U_{front})(U^n_{l,bubble} - U^{n+1}_{l,wave}) = H_{wave}A(P_{J-1} - P_J) + \left(-\frac{1}{8}LS_{l,wave}\lambda_{l,wave}\rho_{l,wave}|U^n_{l,wave}|U^{n+1}_{l,wave}\right) - M_{l,wave}g\sin\theta \quad (19)$$

In the liquid phase, the main component giving pressure variation is the acceleration of the liquid at the wave front. There is also a contribution from liquid wall friction and gravity for the fixed length of the wave front.

Waves fronts are modelled as moving objects similar to slugs but they have a fixed length of 1–2 pipe diameters and move with the wave front velocity. The front velocity of a wave is determined in exactly the same way as for slugs, through a mass balance across the front. Rewriting Eq. (10) in terms of wave quantities gives:

$$U_{front} = \frac{H_{wave}U^{n+1}_{l,wave} - H_{bubble}U^n_{l,bubble}}{H_{wave} - H_{bubble}} \quad (20)$$

where subscript *wave* indicates wave related quantities.

One aim of the wave tracking scheme was to have a simplified model, therefore a simplified wave tail speed relationship was desired. The proposed wave tail speed is one which gives a continuous transition to slug flow, as in the following equation:

$$U_{tail} = C_o U_l \quad (21)$$

A factor of $C_o = 1.2$ allows for continuous transition between wave and slug flow when the liquid holdup in a wave approaches unity, assuming no gas entrained in the slug. Modifications to this relation can be done when gas entrainment is included in the slug.

The mass balance equations in a wave or slug are the same, where the change in mass in a given time step is the difference in mass flux in and out. In contrast to stratified sections, mass in waves and slugs is treated explicitly so that slug length or wave height is consistent with the masses. This is achieved automatically by integrating the wave or slug masses explicitly (Kjølaas, 2007), as in the following equations:

$$\frac{\Delta M_l}{\Delta t} = Flux_{in} - Flux_{out} = \frac{M^n_l(U^{n+1}_l - U_{tail})}{L} - \frac{M^n_l(U^{n+1}_l - U_{front})}{L} \quad (22)$$

$$\frac{\Delta M_g}{\Delta t} = Flux_{in} - Flux_{out} = \frac{M^n_g(U^{n+1}_g - U_{tail})}{L} - \frac{M^n_g(U^{n+1}_g - U_{front})}{L} \quad (23)$$

$$H = \frac{M^{n+1}_l}{AL\rho_l} \quad (24)$$

Eqs. (22) and (23) are the liquid phase and gas phase mass balance equations, respectively, in both slugs and waves. The liquid holdup can then be determined as in Eq. (24). Since wave fronts are modelled with a fixed length and they move at the wave front velocity, the tail velocity only appears in the mass balance equations (22) and (23). If the front speed is larger than the tail speed the liquid mass in the wave will increase and vice versa. Therefore wave fronts can increase or decrease in amplitude. For slugs, if the front velocity is different from the tail velocity, the slug will increase or decrease in length.

A summary of the wave model and quantities determined is given in Table 2.

2.8. Initiation and decay of slugs and waves

In principle, this scheme could be used for capturing wave initiation using the two-fluid model followed by slug tracking similar to Renault (2007) if the grid is sufficiently refined. On a coarser grid in use here, an initiation model for waves is needed. This could be implemented by testing the inviscid Kelvin–Helmholtz (K–H) criterion (Lin and Hanratty, 1986; Barnea and Taitel, 1993) at the transition from stratified flow, as follows:

$$\left(\frac{A_l}{\rho_l S_i} + \frac{A_g}{\rho_g S_i}\right)(\rho_l - \rho_g)g\cos\theta - (U_g - U_l)^2 > 0 \quad (25)$$

Waves can also be inserted in the pipe at a given frequency, as is done here. For testing in this work, they are inserted using experimentally measured frequencies.

The initiation of slugs occurs when the holdup in a wave or the liquid level in a low point exceeds a user specified maximum holdup, for example $H = 0.99$. In that case, the section will be converted to a slug. Slugs can also form if two waves merge or grow if a slug overtakes a slower moving wave.

Slugs are removed either when they exit the pipe or when their length goes below a user specified minimum of one or two pipe diameters, at which point it becomes a wave. If the wave continues to decay, it will be removed when the holdup in the wave approaches the holdup in the stratified section in front of it. This means the wave has decayed in amplitude until it reaches the stratified liquid level surrounding it.

3. Model implementation

The tracking scheme has been developed in the C++ programming language using object oriented techniques. Object oriented programming promotes code reuse through inheritance and enhances modularity which reduce complexity of the program and allow changes to be made more easily. Physical objects such as slugs and waves can be represented as computational objects in the code through the use of classes. Using list structures simplifies the grid management. Equations are also represented computationally using a generic class structure including a mass balance equation class and a momentum balance equation class. The model implementation is discussed in Kjølaas (2007).

3.1. Computational sequence

The mass, momentum, and pressure equations have been formulated implicitly for increased stability and linearized in terms of the unknown primary variables velocity *U*, pressure *P*, and specific mass *m*. The solution is found by using direct Gauss-elimination. The computational sequence is as follows:

1. Equation coefficients for moving borders on wave and slug sections are determined.
2. The pressure and momentum balance equation system matrix is built. This matrix is a banded system with three upper and three lower co-diagonals. The equation system is then solved giving phase velocities and pressures.
3. The mass balance equations are solved with the new velocities.
4. Phase masses, phase densities (state equation), and volume errors are updated.
5. Waves and slugs are inserted or removed, sections are merged and split as necessary.
6. The simulation moves on to the next time step, starting at step 1 again.

3.2. Grid sizes

Modelling on a coarse grid gives square shaped bubbles, slugs, and waves. However, the liquid height profile behind slugs and waves, their tails, can be reproduced by refining the grid in the

stratified region. As this only changes the resolution of stratified sections, the wave and slug velocity computations will not be affected. Fig. 4 shows how an experimental holdup time trace compares to a simulated time trace on a fine (maximum grid size 10 pipe diameters) and on a coarse grid (maximum grid size 100 pipe diameters) at the same conditions. The experiments and simulations were run for an air–water system at atmospheric pressure. The simulation ran considerably faster with the coarse grid compared with the refined grid case.

The minimum slug length corresponds to the short length of a wave front on the order of a pipe diameter. This length will determine the wave front growth rate and how soon slugs decay into waves. The effect of increasing the minimum slug length is that slugs decay to waves sooner, and the growth of wave fronts is delayed. Taking a simulation example with sulfurhexafloride (SF6) gas and water at 8 bar in a 0.1 m I.D. horizontal pipe, Table 3 shows the effect of varying the minimum slug length on the computed wave velocity and average pressure drop. The stratified section length is kept within 8–50 pipe diameters and time step size held below 0.01 s. Increasing or decreasing the minimum slug length by a factor of one or two results in a deviation from the experimental quantities of no more than 8.0%.

The time step in the model is controlled based on the Courant–Friedrichs–Lewy (CFL) condition, in stratified sections which have a stationary grid. The Courant number is as follows:

$$C = U\Delta t/\Delta x \tag{26}$$

where C is the Courant number and Δx is the length of a grid section. C is kept lower than unity for accuracy. The Courant number is tested to see if it reaches unity. If it does, the time step is changed from the user specified value so that C stays below the limit of unity. Taking the same simulation example as above, the typical liquid and gas velocities coming into a stratified grid section are 1.26 m/s and 5.14 m/s, respectively. For a time step of 0.01 s, and a minimum stratified section length of 0.8 m (or 8 pipe diameters), the Courant number for the liquid phase is 0.0158 and for the gas phase is 0.0642.

3.3. Wave and slug dynamics

Wave dynamics such as waves growing to slugs, or slugs decaying to waves is inherent in the tracking model. An example simulation of a wave which grows to a slug and then decays into a wave again is shown in Fig. 5. The pressure variation across the wave, liquid holdup and velocity in the wave object as it moves are plotted against time. When a wave becomes a slug the pressure variation across it and the liquid velocity increase, and the holdup approaches one. When the slug decays again, pressure variation, liquid velocity and holdup decrease. The time traces are cut off when the wave exits the pipe.

Table 3
An example showing the effect of varying minimum slug length on computed values. These values were computed for a 0.1 m internal diameter horizontal pipe at 8 bar with $U_{sg} = 4.5$ m/s and $U_{sl} = 0.2$ m/s. The corresponding experimental wave velocity and average pressure drop were 2.13 m/s and 181.6 Pa/m, respectively, from which percentage differences were calculated.

Minimum slug length (multiple of pipe diameter) (m/s)	Simulated values		Absolute percentage difference (%)	
	Wave velocity (m/s)	Pressure drop (Pa/m)	In wave velocity	In pressure drop
$\frac{1}{2}$	2.2	185	3.3	1.9
1	2.16	189	1.4	4.1
2	2.08	193	2.3	6.3
3	2.0	172	6.1	5.3
4	1.99	167	6.6	8.0

4. Results and discussion

Simulation results from the slug tracking scheme with incorporated wave tracking capability presented above are compared to experimental data (Johnson, 2005) specifically on roll waves.

4.1. Description of experiments

Simulations were run matching the flow conditions, fluid properties, and pipe geometry in Johnson (2005). A total of 984 experiments on two-phase roll waves were carried out at the Institute for Energy Technology (IFE) in Norway using sulfurhexafloride gas and water at 8 bar and 20 °C to simulate high pressure flows (Johnson, 2005). Pipe inclinations varied from 0 to 5 deg with gas superficial velocities, U_{sg}, ranging between 0.5 and 4.5 m/s and a variety of liquid superficial velocities, U_{sl}, in the range of 0.1–0.6 m/s at each inclination and U_{sg}. The test section was 25 m long, internal pipe diameter was 0.1 m and experiments ran for 100 s.

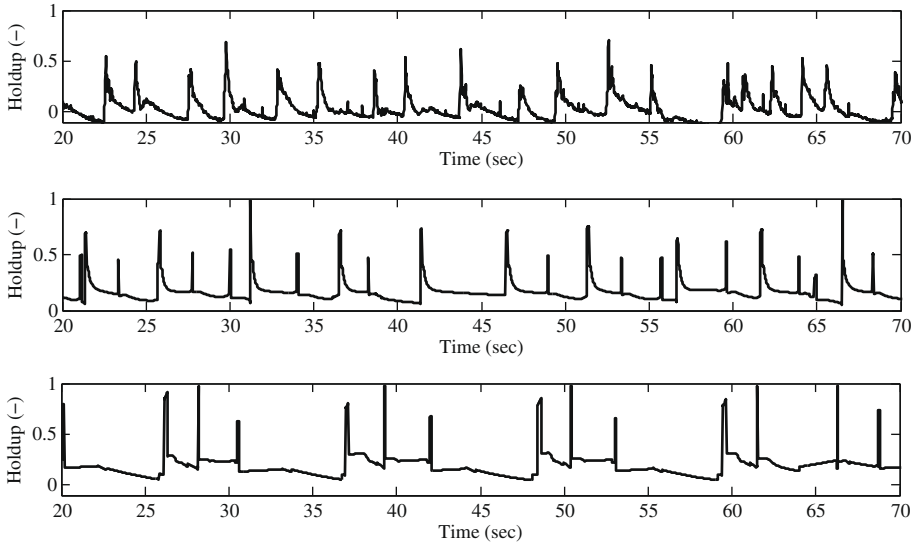

Fig. 4. Liquid holdup time traces using air and water at atmospheric pressure in a 0.06 m internal diameter pipe (De Leebeeck and Nydal, 2009). Top: experimental. Middle: simulated on a fine grid (length 10 pipe diameters). Bottom: a coarse grid (length 100 pipe diameters). $U_{sg} = 6.09$ m/s, $U_{sl} = 0.18$ m/s, $\theta = 2$ deg.

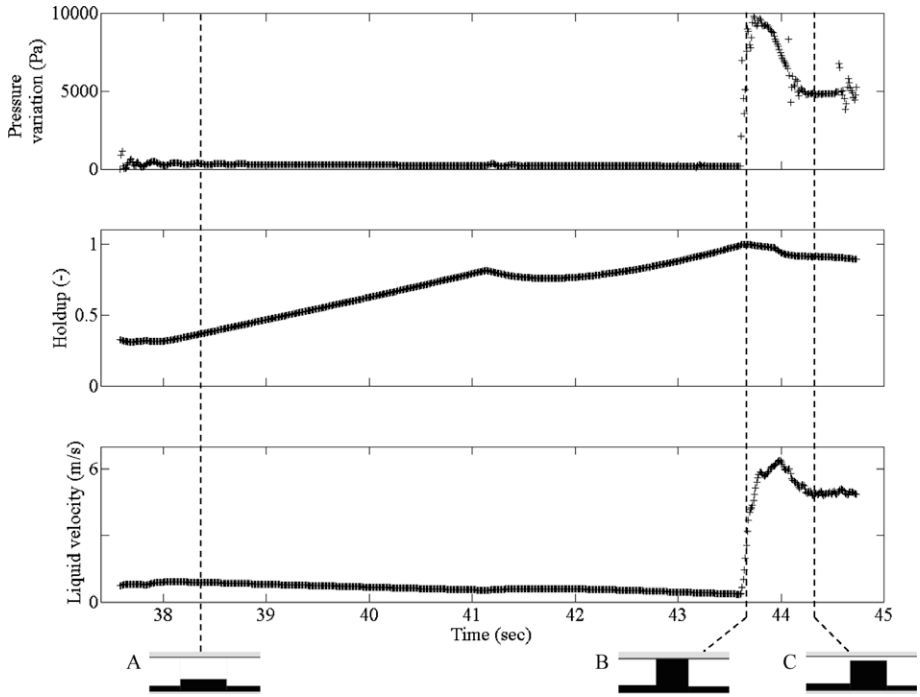

Fig. 5. Pressure variation, liquid holdup, and liquid velocity in a wave vs. time for (A) a wave growing to (B) a slug and then decaying to (C) a wave again. Simulation run at atmospheric pressure with $U_{sg} = 5.87$ m/s, $U_{sl} = 0.13$ m/s, $\theta = 1$ deg, and pipe internal diameter 0.06 m (De Leebeeck and Nydal, 2009).

The gas density and viscosity were 50 kg/m^3 and 1.61×10^{-5} Pa s, and water density and viscosity were 998 kg/m^3 and 1×10^{-3} Pa s, respectively.

The data available from the experiments included average pressure drops, superficial velocities, average liquid height, wave velocities, the length from one wave peak to the next, and wave amplitudes. Wave velocities were obtained from cross correlations between liquid height time traces. Peak to peak lengths were estimated from the dominant wave frequency and the wave velocity. Experimental results of interest for comparison with the present numerical model were in particular the wave speed and average pressure drop.

4.2. Simulations

Simulations were run using the same conditions as above. The model domain was 25 m long and each simulation was run for 100 s. Measured superficial velocities were set at the inlet boundary and the inlet source gas density was determined at 8 bar from the ideal gas law. The pressure at the outlet boundary was set to 8 bar. Various U_{sl} and U_{sg} combinations were simulated at four pipe inclinations: 0, 0.1, 0.25 and 1 deg. Grid sizes were as follows: the minimum slug length was one pipe diameter, the minimum stratified section length was 8 pipe diameters and the maximum length was 50 pipe diameters. A time step of 0.01 s was specified.

Waves were inserted at the dominating frequency determined in experiments. This frequency in combination with the wave velocity was used to find the experimental length between subsequent wave peaks but was not explicitly listed in Johnson (2005). Using the given wave velocity and experimental length, the wave frequency was calculated and used to specify a time delay between wave front insertions in the simulation. For example, the experimental case $U_{sg} = 4.5$ m/s, $U_{sl} = 0.2$ m/s, with pipe inclined at 0 deg has a corresponding length between subsequent wave peaks of 2.42 m and wave speed of 2.13 m/s (Johnson, 2005). The experimental length L_{expr} is determined as follows, knowing both dominating frequency f_d, and experimental wave velocity U_{wave} (Johnson, 2005):

$$L_{expr} = \frac{U_{wave}}{f_d} \tag{27}$$

For the stated example, the dominating frequency was 0.88 Hz or a delay of 1.1 s between waves. In the simulation of this case, waves were inserted close to the inlet every 1.1 s.

A sampling of 65 experiments were chosen as examples to compare to simulations. Simulations could have been run for all the experiments conducted but this would have been time consuming since nearly 1000 experiments were made. The smaller selection covers a range of U_{sg}, U_{sl}, and pipe inclinations summarized in Table 4. The velocities U_{sl} and U_{sg} for a given experimental case are summed together to obtain the mixture velocity, which is used in later plots.

4.3. The discharge coefficient C_d

Estimating C_d has been one of the challenges of simplification in this model. C_d is an open parameter in the simplified model using an orifice type relation that needs to be chosen. A test case with $U_{sg} = 4.5$ m/s and $U_{sl} = 0.2$ m/s in a horizontal pipe was used to determine the model's sensitivity to various values of C_d. These results are listed in Table 5. For reference, the experimentally determined wave velocity is 2.13 m/s and the pressure drop is 181.6 Pa/m. The results indicated that if C_d was doubled to 0.8 or

Table 4
Cases simulated.

Inclination (deg)	U_{sl} (m/s)	U_{sg} (m/s)
0	0.2, 0.4	1.0, 1.5, 2.0, 2.5, 3.0, 3.5, 4.0, 4.5
0.1	0.2, 0.25, 0.35, 0.4	1.0, 1.4, 1.8, 2.2, 2.6, 3.0, 3.5, 4.0, 4.5
0.25	0.2, 0.3, 0.4	1.6, 1.8 2.2, 2.4, 2.6, 3.0, 3.5, 4.0, 4.5
1	0.1, 0.2, 0.3	2.0, 2.5, 3.0, 3.5, 4.0, 4.5

Table 5
Simulated wave velocity and pressure drop for different values of discharge coefficient C_d. Simulations were run for a 0.1 m internal diameter horizontal pipe at 8 bar with $U_{sg} = 4.5$ m/s and $U_{sl} = 0.2$ m/s.

Discharge coefficient C_d	Wave velocity (m/s)	Pressure drop (Pa/m)
0.2	2.72	234
0.4	2.16	189
0.6	1.88	165
0.8	1.66	155

halved to 0.2, wave velocity and pressure drop varied by about 25%. The wave velocity and pressure drop calculated with $C_d = 0.4$ gave the most reasonable approximation to the experimental values and so $C_d = 0.4$ has been used for all other simulations.

4.4. Wave velocities

A comparison of the experimental and simulated wave velocities was made. These are plotted against the mixture velocity $(U_{sl} + U_{sg})$ in four separate graphs for each pipe inclination in Fig. 6. Since two or three different U_{sl} values in combination with a wider range of U_{sg} were simulated, there appears to be two or more data sets in each plot. For similar mixture velocities, a larger wave velocity corresponds to a larger U_{sl} value. The experimental wave speeds were smaller than the mixture velocity whereas slug velocities would be approximately 1.2 times the mixture velocity. The tracking scheme reproduced waves with velocities of the expected magnitude, that is, less than what the bubble nose velocity of a slug would be for a given U_{sg} and U_{sl} combination.

The average absolute percentage difference between model and experiment was 8.4% with maximum difference of 43% and minimum of 0.36%. There were 56 of 65 total simulated wave speeds within 20% of the experimental values, indicating good agreement. The simulated case with the largest percentage difference belonged to pipe inclination 1 deg, $U_{sg} = 2.5$ m/s, and $U_{sl} = 0.3$ m/s. Most of the waves inserted in this simulation grew to slugs. The velocity used in the percentage difference estimation was the average velocity of waves before they grew to slugs, this result is slower than what was measured experimentally. Considering the simplicity of the model, the comparison with experimental wave speeds are good.

4.5. Pressure drops

It has been observed experimentally that pressure drop in flow with large amplitude waves increases significantly compared to smooth stratified flow (Holmås, 2008; Espedal, 1998; Fernandino, 2007). Considering the assumptions in the tracking scheme, it is also expected that pressure drop will increase with the number of waves in the pipe and that if slug flow occurs pressure drop will be larger still. For comparison, a case at horizontal, $U_{sg} = 3.5$ m/s, $U_{sl} = 0.2$ m/s with a wavelength of 2.65 m corresponding to a delay of 1.5 s between waves gives an averaged pressure drop of 119 Pa/m compared with an experimental value of 121.7 Pa/m

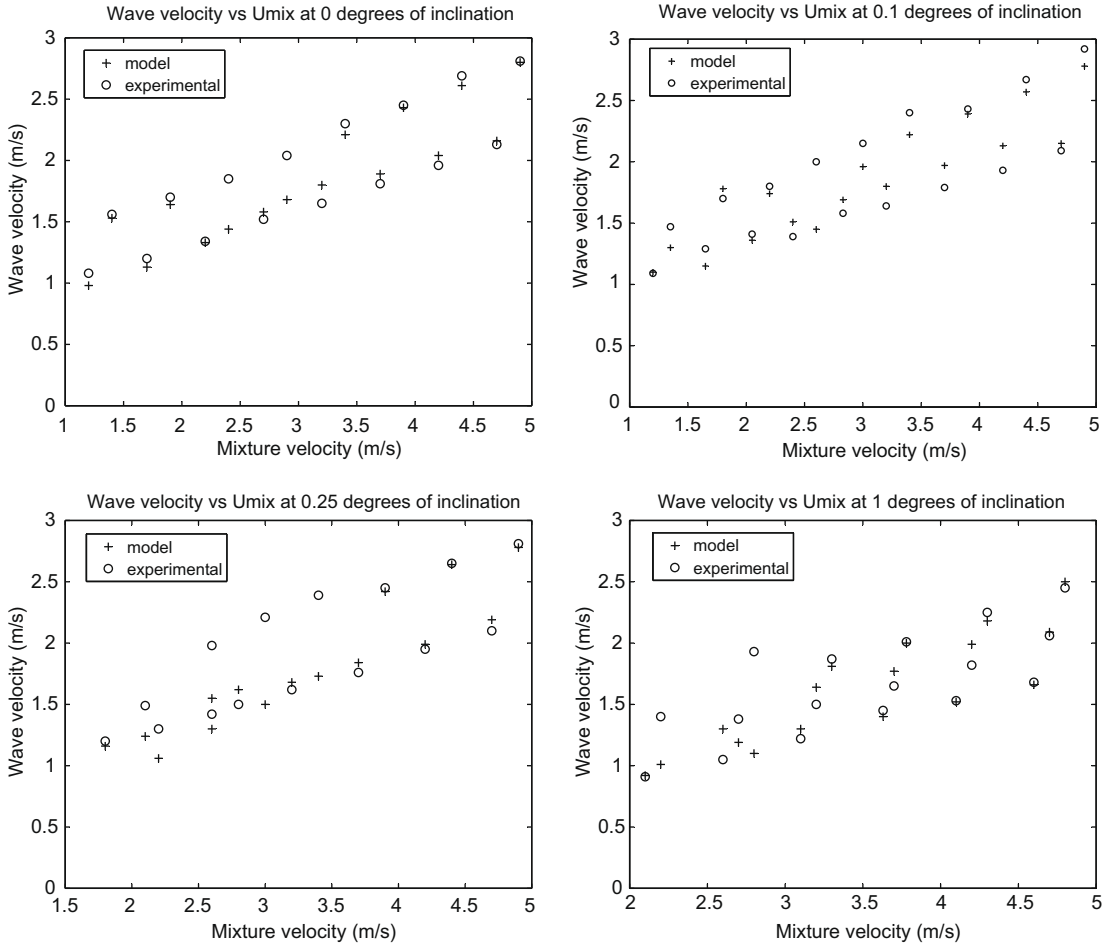

Fig. 6. Experimental wave velocities (Johnson, 2005) compared with results from dynamic tracking simulations.

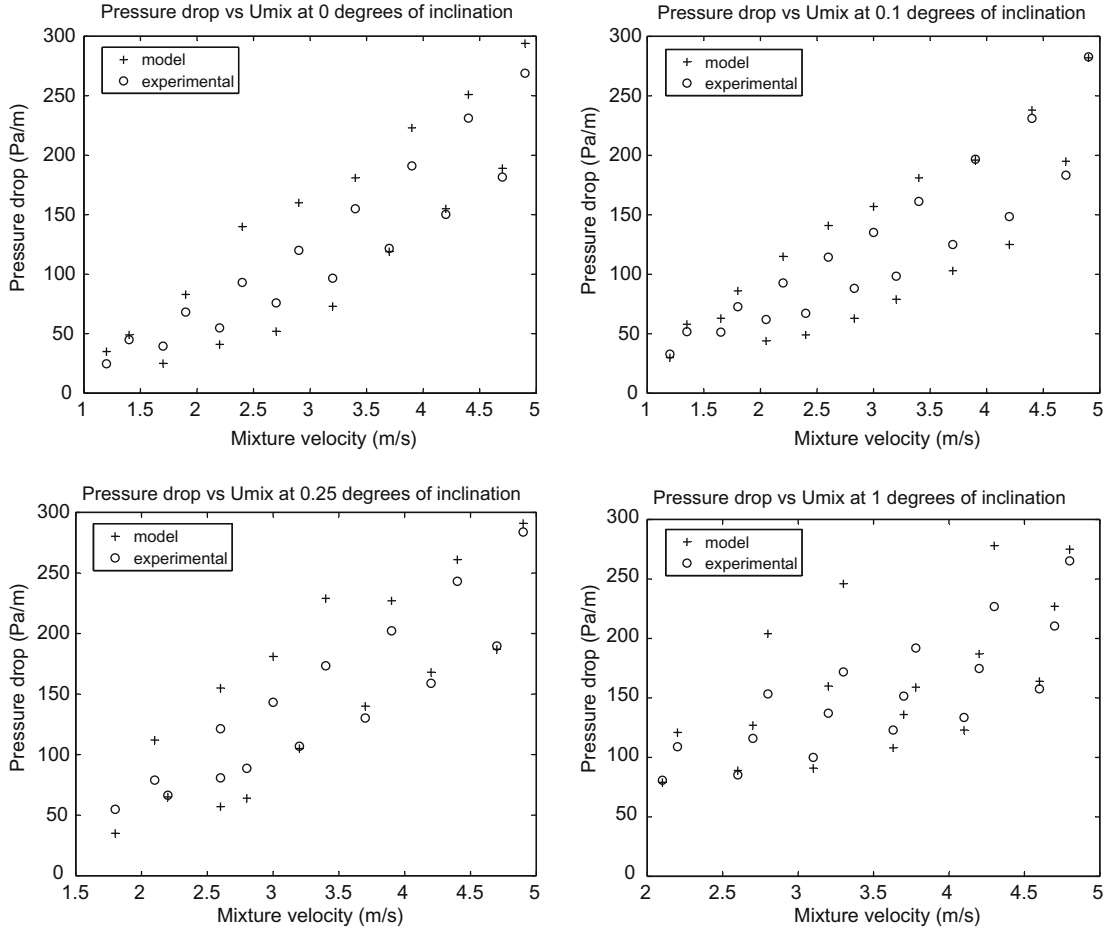

Fig. 7. Experimental pressure drops (Johnson, 2005) compared with averaged pressure drops from tracking simulations.

(Johnson, 2005), but with stratified flow (infinite time delay between waves) the pressure drop is 68 Pa/m.

Experimental pressure drops and averaged pressure drops from the tracking scheme are compared in four separate graphs for each pipe inclination in Fig. 7. As in Fig. 6, there appears to be two or more data sets in each plot. For similar mixture velocities, higher pressure drops correspond to larger U_{sl}. The model predicted pressure drops quite well, with an absolute percentage difference of 17% on average, minimum of 0.29% and maximum of 50%. Two thirds of the modelled data points were within 20% of the experimental data. In the case of the largest deviation in a horizontal pipe with $U_{sg} = 2$ m/s and $U_{sl} = 0.4$ m/s, some of the simulated waves grew to slugs. Since slugs occurred the modelled pressure drop, 140 Pa/m was larger than the experimental 93 Pa/m (Johnson, 2005). Some of the pressure predictions could be larger than expected because waves appeared too frequently in the simulation, or because some of them grew to slugs.

5. Conclusions

A simplified model for large amplitude roll waves has been implemented and tested in a dynamic slug tracking scheme. The wave model includes a simple relation for wave speed which allows for a smooth transition to slug flow. Pressure variation across wave fronts is modelled with a modified orifice type relation. The model predicts wave velocities which are less than slug velocities and pressure drops larger than in the case of stratified flow.

Dynamic flow simulations have been compared with available experimental data for roll waves at high gas densities. The waves in the simulations were initiated with a frequency similar to the experimental frequencies. The resulting comparison between computed wave velocities and pressure drops were good with average percentage differences of 8.4% and 17%, respectively. The quality of wave and slug tracking simulations depends on the initiation models. It remains as a challenge to develop grid independent initiation models for wave and slug tracking on a coarse grid.

Acknowledgment

Financial support from Total E&P Norge is gratefully acknowledged by A. De Leebeeck.

Appendix A. Supplementary data

Supplementary data associated with this article can be found, in the online version, at doi:10.1016/j.ijmultiphaseflow.2009.09.002.

References

Andreussi, P., Bonizzi, M., Lullo, A.D., Margarone, M., Scotti, A., Taddei, S., 2008. Advanced simulation of gas–liquid pipelines. In: Proceedings of the Sixth North American Conference on Multiphase Technology, Banff, Canada.

Andritsos, N., Hanratty, T.J., 1987. Interfacial instabilities for horizontal gas–liquid flows in pipelines. Int. J. Multiphase Flow 13, 583–603.

Barnea, D., Taitel, Y., 1993. Kelvin–Helmholtz stability criteria for stratified flow: viscous versus non-viscous (inviscid) approaches. Int. J. Multiphase Flow 19, 639–649.

Bendiksen, K.H., 1984. An experimental investigation of the motion of long bubbles in inclined tubes. Int. J. Multiphase Flow 10, 467–483.
Bendiksen, K.H., Malnes, D., Nydal, O.J., 1996. On the modelling of slug flow. Chem. Eng. Commun. 141–142, 71–102.
Bonizzi, M., Issa, R.I., 2003. A model for simulating gas bubble entrainment in two-phase horizontal slug flow. Int. J. Multiphase Flow 29, 1685–1717.
De Leebeeck, A., Gaarder, A.H., Nydal, O.J., 2007. Experiments on roll waves in air–water pipe flow. In: 16th Australasian Fluid Mechanics Conference, Gold Coast, Australia.
De Leebeeck, A., Nydal, O.J., 2009. Large amplitude waves in a slug tracking scheme. In: Mammoli, A.A., Brebbia, C.A. (Eds.), Computational Methods in Multiphase Flow V. WIT Press, New Forest, UK, pp. 99–110.
Espedal, M., 1998. An experimental investigation of stratified two-phase flow at small inclinations. Ph.D. Thesis, Norwegian University of Science and Technology.
Fernandino, M., 2007. Experimental and numerical characterization of turbulence structure in stratified horizontal air water duct flow. Ph.D. Thesis, Norwegian University of Science and Technology.
Ferziger, J.H., Perić, M., 2001. Computational Methods for Fluid Dynamics, third ed. Springer-Verlag, Berlin.
Fletcher, D.F., Thyagaraja, A., 1991. A finite difference error arising from the use of a staggered grid. Appl. Math. Model. 15, 496–498.
Haaland, S., 1983. Simple and explicit formulas for the friction factor in turbulent pipe flow. J. Fluid Eng. 105, 89–90.
Hanyang, G., Liejin, G., 2008. Experimental investigation of slug development on horizontal two-phase flow. Chin. J. Chem. Eng. 16, 171–177.
Holmås, H., 2008. Numerical simulation of waves in two-phase pipe flow using 1D two-fluid models. Ph.D. Thesis, University of Oslo.
Hu, B., Stewart, C., Manfield, P.D., Ujang, P.M., Hale, C.P., Lawrence, C.J., Hewitt, G.F., 2007. A model for tracking the evolution of slugs and waves in straight pipelines. In: Sixth International Conference on Mulitphase Flow, Leipzig, Germany.
Issa, R.I., Kempf, M.H.W., 2003. Simulation of slug flow in horizontal and nearly horizontal pipes with the two-fluid model. Int. J. Multiphase Flow 29, 69–95.
Johnson, G.W., 2005. A study of stratified gas–liquid pipe flow. Ph.D. Thesis, University of Oslo.
Kjølaas, J., 2007. Plug propagation in multiphase pipelines. Ph.D. Thesis, Norwegian University of Science and Technology.
Lin, P.Y., Hanratty, T.J., 1986. Prediction of the initiation of slugs with linear stability theory. Int. J. Multiphase Flow 12, 79–98.
Lin, P.Y., Hanratty, T.J., 1987. Detection of slug flow from pressure measurements. Int. J. Multiphase Flow 13, 13–21.
Nydal, O.J., Banerjee, S., 1996. Dynamic slug tracking simulations for gas–liquid flow in pipelines. Chem. Eng. Commun. 141–142, 13–39.
Ottens, M., Klinkspoor, K., Hoefsloot, H.C.J., Hamersma, P.J., 2001. Correlations predicting liquid hold-up and pressure gradient in steady-state (nearly) horizontal co-current gas–liquid pipe flow. Trans. IChemE 79, 581–592.
Prosperetti, A., Tryggvason, G., 2007. Computational Methods for Multiphase Flow. Cambridge University Press, Cambridge.
Renault, F., 2007. A Lagrangian slug capturing scheme for gas–liquid flows in pipes. Ph.D. Thesis, Norwegian University of Science and Technology.
Soleimani, A., Hanratty, T., 2003. Critical liquid flows for the transition from the pseudo-slug and stratified patterns to slug flow. Chem. Eng. Sci. 29, 5167.
Taitel, Y., Barnea, D., 1998. Effect of gas compressibility on a slug tracking model. Chem. Eng. Sci. 53, 2089–2097.
White, F.M., 2005. Fluid Mechanics, fifth ed. McGraw-Hill, Boston.